BACHELOR

Accelerated target capture at a sensor surface by microfluidic stirring with magnetic particles

Mackaij, M.B.

Award date:
2013

Accelerated target capture at a sensor surface by microfluidic stirring with magnetic particles

Maarten Mackaij

MBx 2013-02

Abstract

For this project, the influence of microfluidic stirring with magnetic particles on the binding speed of targets in a biosensor is studied. As a model system for the biosensor, a fluid cell is used with biotin-coated polystyrene fluorescent particles functioning as targets. These fluorescent particles bind to a streptavidin-coated surface at the bottom of a fluid cell. Actuation is performed by applying a vertically rotating magnetic field to superparamagnetic particles suspended in the fluid. The field causes the particles to form rotating chains, which agitate the fluid.

The main parameter that is studied is the number of particles that are bound to the bottom of a fluid cell after a certain time. This is done for the case where the movement of particles is purely caused by diffusion and for the case where stirring with magnetic chains was present. It is found that stirring enhances the binding speed of particles by a factor of approximately 2.5 times.

Different actuation protocols were applied. The main parameters that were varied were the magnetic field strength and the frequency of the rotating magnetic field. It is found that varying these parameters influences the number of particles that bind.

Explanations for differences in the number of bound particles for various actuation protocols were found by characterizing the chain behavior during actuation protocols. This was done by making movies of the chains during actuation. An example of a result found from these movies is that clustering of chains led to a lower stirring efficiency.

A more in-depth analysis for the results was provided with a numerical model. In this model, a fluid cell filled with particles is simulated. The motion of each particle is calculated according to Brownian dynamics. Stirring with magnetic chains was implemented in a simplified way in this model: by randomizing target distributions in a subvolume. The model calculates the number of particles bound to the bottom surface of the fluid cell. For measurements where no stirring was present, the model showed the same square root time dependency for the number of bound particles as the experimental data. If the number of bound particles calculated with the simulation model is compared to the experimental data for the measurements where the magnetic field strength is varied, the model shows different behavior than the experiments. In the model, the number of bound particles increases with the field strength, while in the experimental data increasing the field strength does not increase the number of bound particles. This may be caused by an infinite binding speed of particles to the surface in the model. In reality, the binding speed is not infinite and may limit the number of particles that can bind after a certain time.

In this project, it is found that microfluidic stirring influences the binding speed of targets in a fluid cell. In general, stirring enhances the binding speed. Different actuation protocols led to different stirring efficiencies and explanations can be found when characterizing the chain behavior.

Table of contents

1 Introduction

Biosensors are used in medical diagnostics to detect biological molecules in for example blood or urine. Detection of certain molecules provides important medical information, for example if the patient suffers a high risk for a heart attack.

To measure biological molecules, or targets, in a biosensor, multiple steps are needed. First, some body fluid needs to be inserted into the biosensor. After that, the targets need to be bound from the fluid to a signal transducer (i.e. a surface) in the biosensor. When the targets are located on the transducer and perhaps labeled, the biosensor will be able to detect them and determine the target concentration in the sample fluid.

The challenge is to increase the sensitivity of biosensors so far that they are able to detect very low target concentrations, like nanomolar/femtomolar range, in combination with low measurement times. The lower the target concentration, the fewer particles will bind to the sensor surface. Therefore, measuring targets in the nanomolar/femtomolar range takes more time than measuring at higher target concentrations, like the millimolar range for glucose for example.

To speed up biosensors, the Molecular Biosensors for Medical Diagnostics group at Eindhoven University of Technology, where this research project is performed, is researching technologies to enhance the binding speed of targets to a sensor surface. For this project, the influence of stirring the fluid with mesoscopic particles is studied.

To model the biosensor, a fluid cell is used. In this fluid cell, particles coated with biotin function as the target particles. The bottom of the fluid cell is coated with streptavidin. These two particles are chosen because the attractive interaction between them is very high: once a target is bound, it will probably stay bound.

The microfluidic stirring is done with superparamagnetic particles. These particles form chains when they are exposed to a magnetic field. The magnetic field is rotating in the vertical plane which causes the chains to rotate in this plain as well.

The goal of this project is to study the effect of different stirring methods on the binding speed of target particles. Varying stirring methods are applied by changing the magnetic field strength and frequency. The effectiveness of the method is quantified by the number of targets bound to the surface of the fluid cell as a function of time.

2 Theory

The goal of this project is to study the effect of different stirring methods on the binding speed of target particles. Here, a theoretical background is provided to help with this analysis. First, an analytical expression is derived from the diffusion equation for the number of bound particles at a surface as a function of time. This provides us information about the binding speed of targets when only diffusion is present. Then, the chain behavior during stirring is analyzed by introducing the Mason number and its influence on the chain length.

2.1 Analytical expression for number of bound particles at a surface

By using the diffusion equation, also called Fick's second law, an expression is found for the number of particles binding to a surface when only diffusion causes the particles to move. This expression is shown in equation 1. A derivation of equation 1 is shown in appendix D.

$$Bound\ particles = Ap_{\infty}N_A\sqrt{\frac{4Dt}{\pi}} \tag{1}$$

where A is the area the particles can bind to in m², p_{∞} the particle concentration at time t = 0 in mol/m³, N_A Avogadro's number in mol^{-1}, D the diffusion coefficient in m²/s and t the time in s.

Fick's second law describes the motion of particles as a function of time if only diffusion causes movement of the particles. If this situation is applied to a fluid cell, the number of particles passing through a surface of the volume cell can be calculated (given initial parameters like the initial particle concentration). Equation 1 actually calculates the number of particles passing through a surface. But by using the assumption that all particles passing through the surface bind to the surface, an expression for the number of bound particles is found.

2.2 Behavior of magnetic particle chains in a rotating magnetic field

For a single rotating chain in a bulk fluid the ratio of viscous forces to magnetic forces can be defined. To define this ratio, the system needs to be in a Stokes regime. In a Stokes regime, the Reynolds number is low, which causes the instationary term in the Navier-Stokes equation to vanish. The viscous forces of the fluid on the chain will lead to break up behavior of the chain, while the magnetic forces keep the chain together. The ratio of these forces is called the Mason number, and is defined in equation 2 [1]. Typical Mason numbers are in the order of 0.001 in size. This is in case of a single chain in a bulk fluid however, and cannot be directly compared to situations present in this project.

$$\mathrm{Ma} = \frac{\eta\omega}{\mu_0\chi_p H_0^2} \tag{2}$$

where Ma is the Mason number, $\eta\omega$ the characteristic pressure with ω being the frequency of the rotating magnetic field, μ_0 the vacuum permeability, χ_p the magnetic susceptibility of the particles and H_0 the magnetic field intensity.

Since the Mason number is the ratio of viscous forces to magnetic forces, chains exhibit more breaking behavior for higher Mason numbers. This is because the hydrodynamic drag is large compared to the dipole-dipole interactions keeping the chains together. This way, chains become shorter in length for higher Mason numbers.

3 Experimental setup

This chapter first discusses the components used during experiments, starting with the fluid cell and its contents and thereafter the microscope and relevant settings used during experiments. After that, the magnetic setup used for actuation of magnetic particles is discussed. Furthermore, the working of the simulation model used to analyze experimental results is shortly discussed at the end of this chapter. Parameters used in the model are also provided there.

3.1 Fluid cell and materials used

A fluid cell is used during this project as a model system for a biosensor. The fluid cell is cylindrical in shape with a height of 700 micrometer and a diameter of 9 millimeter. The exact solution present in the fluid cell can be found in appendix A2. This paragraph will briefly describe the most important parts in the fluid cell. A schematic view of the fluid cell is shown in figure 1.

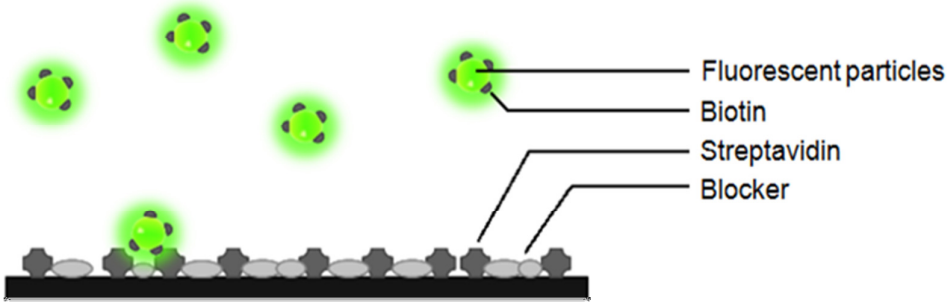

Figure 1: Schematic view of the fluid cell used.

Fluorescent polystyrene particles coated with streptavidin are used to model targets in a biosensor. The particles are fluorescent so they can be easily seen under fluorescent light with a microscope. The diameter of the fluorescent particles is 0.2 micrometer.

Biotin and streptavidin are both proteins with one of the largest non-covalent attractive interactions in biology [2]. The equilibrium constant of this interaction is 10^{15} M^{-1}. Because of the large attractive interaction between biotin and streptavidin, it is unlikely bound particles will be unbound again. The bottom of the fluid cell is coated with streptavidin. This way, the coated fluorescent particles bind to the bottom of the fluid cell and will likely not be unbound during the measurements.

When magnetic stirring is applied, superparamagnetic particles (Dynaparticles-M270) with a diameter of 2.83 micrometer are added to the fluid cell. A schematic drawing of the particles is shown in figure 2. The particles consist of a polystyrene shell filled with magnetite grains. The typical size of these grains is 6 to 12 nm. If a magnetic field is applied, the magnetic moments of all the grains will align. This causes dipole-

dipole interactions to form between the particles. Because of this, the particles are attracted to each other and form chains that are aligned to the applied magnetic field.

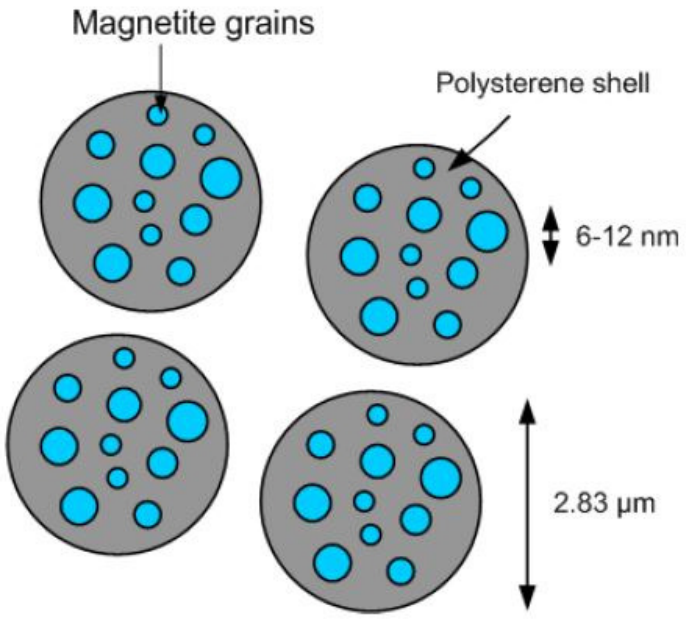

Figure 2: Schematic view of the superparamagnetic particles used in the experiments.

3.2 Microscope

The microscope used in the experiments is a Leica DM6000 upright microscope. The camera attached to the microscope is an Andor Luca S camera. Measurements are done by using the fluorescent lamp in combination with the FLUO L5 filtercube. This way, the fluorescent targets in the fluid cell become visible on the camera. The aperture of the microscope is set to maximum value for all measurements. The software used to operate the camera is Andor SOLIS.

When the number of particles that bind to the bottom of the fluid cell is measured, the following settings are used in the Andor SOLIS software.

- Mode: accumulate
- Exposure time: 0.1 s
- Number of accumulations: 10
- Cycle time: ~7 Hz
- Total magnification: 630 x

Measurements are saved as Andor Data File (.sif) and then converted to a bitmap image (.bmp). Accumulation mode is used to prevent moving particles from showing up as bound particles. If a particle is bound, it lights up in multiple images and in this way produce a bright spot. Moving particles will only produce weak spots at multiple locations. By using a threshold during the image analysis (performed with ImageJ), bound particles can be filtered from moving particles.

When the microscope is used to view the magnetic chains during actuation, the following settings are used in the Andor SOLIS software.

- Mode: kinetic
- Kinetic series length: 500 frames
- Total magnification: 200 x

Measurements are saved as Andor Data File (.sif) and then converted to an .avi file. The .avi files can directly be studied with image analysis software (ImageJ in this case).

3.3 Magnetic setup

The magnetic setup used to create vertically rotating chains of magnetic particles is shown in figure 3. It consists of five electromagnets in total. Four of these are positioned in the horizontal plane, the fifth magnet is positioned to the bottom of these four. There are three magnetic poles necessary to create a vertical rotating magnetic field. This is schematically shown in figure 3 (a). Figure 3 (b) shows a photo of the used magnetic setup. The four magnets in the horizontal plane are used to redisperse the magnetic particles during actuation. Finally, figure 3 (c) shows how the fluid cell is placed in the magnetic setup during actuation. It is positioned in the middle of the four horizontal magnetic poles. The vertical placement of the fluid cell is shown in figure 3 (a).

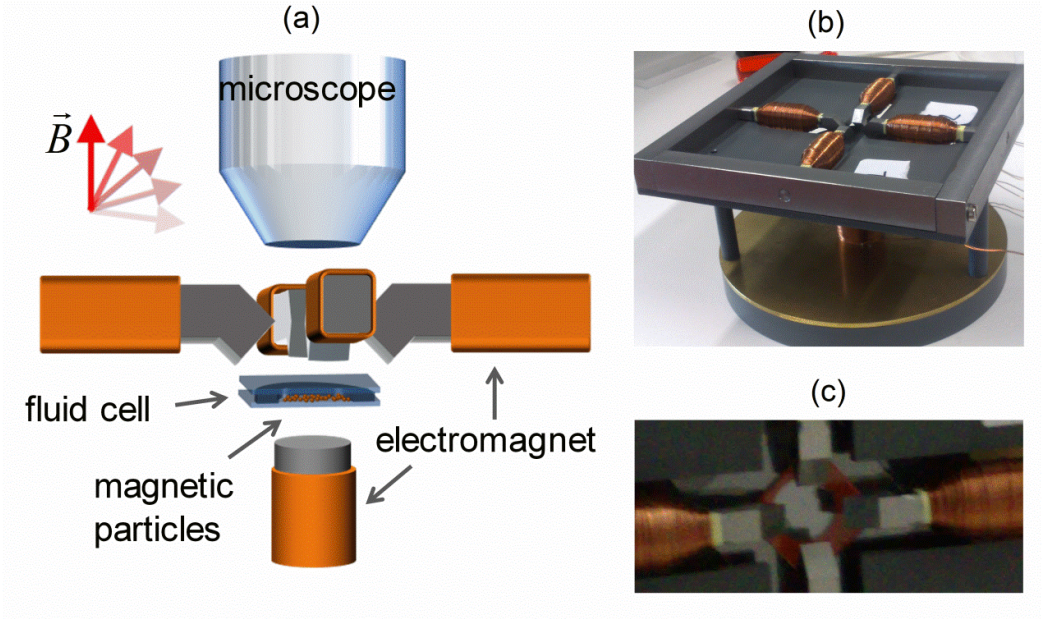

Figure 3: A schematic view of the magnetic setup is shown in figure (a). Figure (b) shows a photo of the magnetic setup used. Figure (c) shows a close-up (taken from above) of the fluid cell in the magnetic setup.

Each of the electromagnets shown in figure 3 can be operated separately. The software used to operate the electromagnets can regulate the current that goes through a coil and the phase difference between the currents through different coils. By varying these parameters magnetic fields with different field strength and different rotational frequency can be applied.

3.4 Simulation model

To analyze experimental results, the binding process of target particles to a reactive surface was modeled numerically, by using Matlab. Using this model, the number of particles that bind to a surface at a given time can be studied under different circumstances. The motion of the particles is treated as Brownian dynamics [3]. In the first time step, particles are distributed randomly across the fluid cell. After that, the script calculates the next position for all the particles according to Brownian dynamics. Boundary conditions are implemented as well when the new position of the particles is outside the boundaries of the fluid cell. If a particle reaches a position with a negative z-coordinate (to the bottom of the capture surface), the particle can be bound depending on the binding probability. Bound particles are counted and removed from the simulation.

The stirring effect of magnetically actuated chains was implemented in the model as well. This was done by homogenizing the particle concentration in a subvolume of the fluid cell at certain time intervals. The height of the subvolume is equal to the chain length because the chains rotate in the vertical plane during actuation. The actuation step can be repeated at certain time intervals to simulate an actuation protocol. These time intervals depend on the rotation frequency of the magnetic field. Implementing the effect of stirring in this way is a simplification of stirring in a real fluid cell.

The parameters in the simulation are matched to the fluid cells used in the experiments. The most important parameters are listed below.

- Height: 700 micrometer
- Width and length: 100 micrometer
- Particle concentration at start of simulation: 0.75 pM
- Number of particles at start of simulation: 3160

The particle concentration is calculated from the protocols found in appendix A2. The calculation is done by taking the particle concentrations in stock solutions and then taking into consideration the steps followed by the protocol.

The complete simulation model along with a more detailed description can be found in appendix C.

4 Results and discussion

Here, the results of the capture measurements will be presented. The main parameter that was measured is the number of particles that bind after a certain time to the bottom of the fluid cell. Firstly, the number of bound particles was measured when no stirring is present. These measurements are called passive measurements. After that, different types of stirring are applied. For these measurements, the number of bound particles after a certain time was measured. To analyze the data in more detail, experiments were performed to characterize the chain behavior during actuation, but also numerical simulations were executed.

4.1 Passive measurements

Capture of targets by a sensor surface was studied without any actuation, i.e. capture was performed passively by diffusion of target particles alone. To quantify target capture, the number of particles that bind to the bottom of the fluid cell was studied. The results of the passive measurements are also used to validate the simulation model discussed in paragraph 3.4 and appendix C.

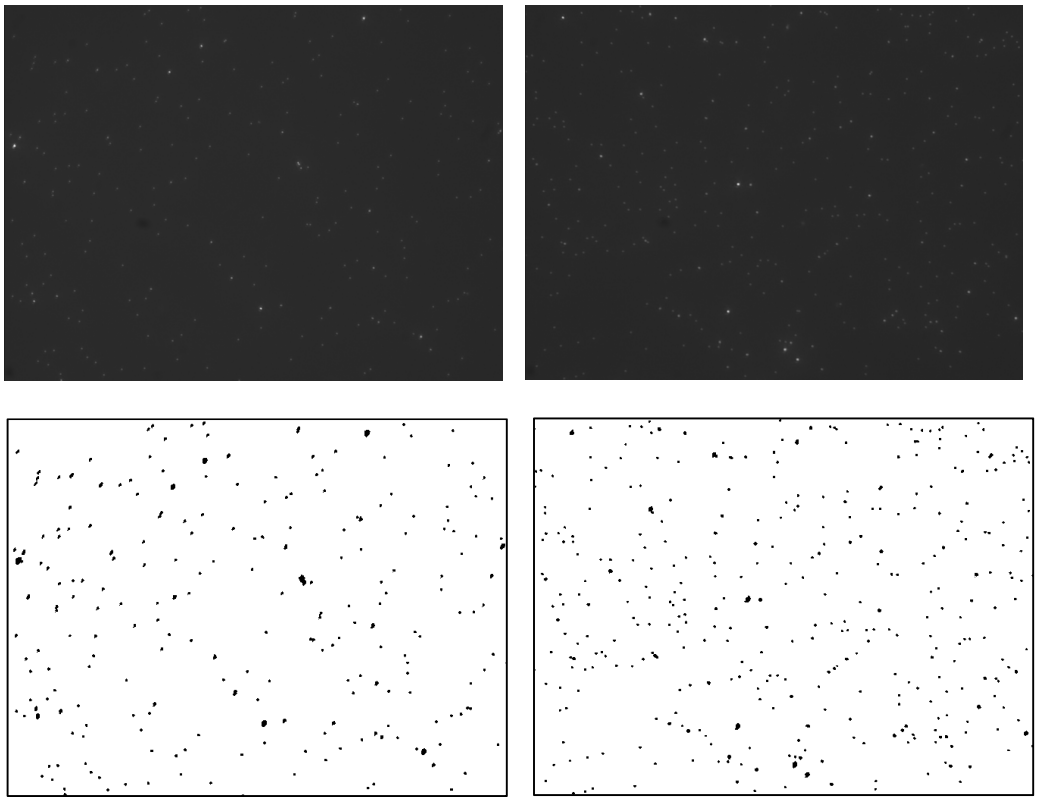

Figure 4: Microscope images of the bottom of the fluid cell before (upper images) and after (lower images) image processing. The pictures on the left are made at t = *900 s and the images on the right are made at* t = *3840 s. The dimensions of the pictures are 0.15 x 0.10 mm. The target concentration at the start of the experiment is 0.75 pM.*

The number of particles on the bottom of the fluid cell is measured by monitoring the

streptavidin-coated surface at the bottom of the fluid cell through a microscope. As an example, two images are displayed in the upper part of figure 4. The image on the left is taken at t = 900 s, the image on the right at t = 3840 s. Both images originate from a measurement series on the same fluid cell. In a typical experiment, images are taken from random spots within the fluid cell. This way, multiple locations of the fluid cell surface are analyzed in one measurement series. Image processing is then applied to count the number of bound particles. During image processing, a bandpass filter is applied to remove small gradients in the image and a threshold is used to filter out the bound particles. How the images look after image processing is visible in the lower part of figure 4.

The number of bound particles for the measurements without actuation is shown in figure 5. Error bars in the particle count are caused by the analysis method (as described in appendix B).

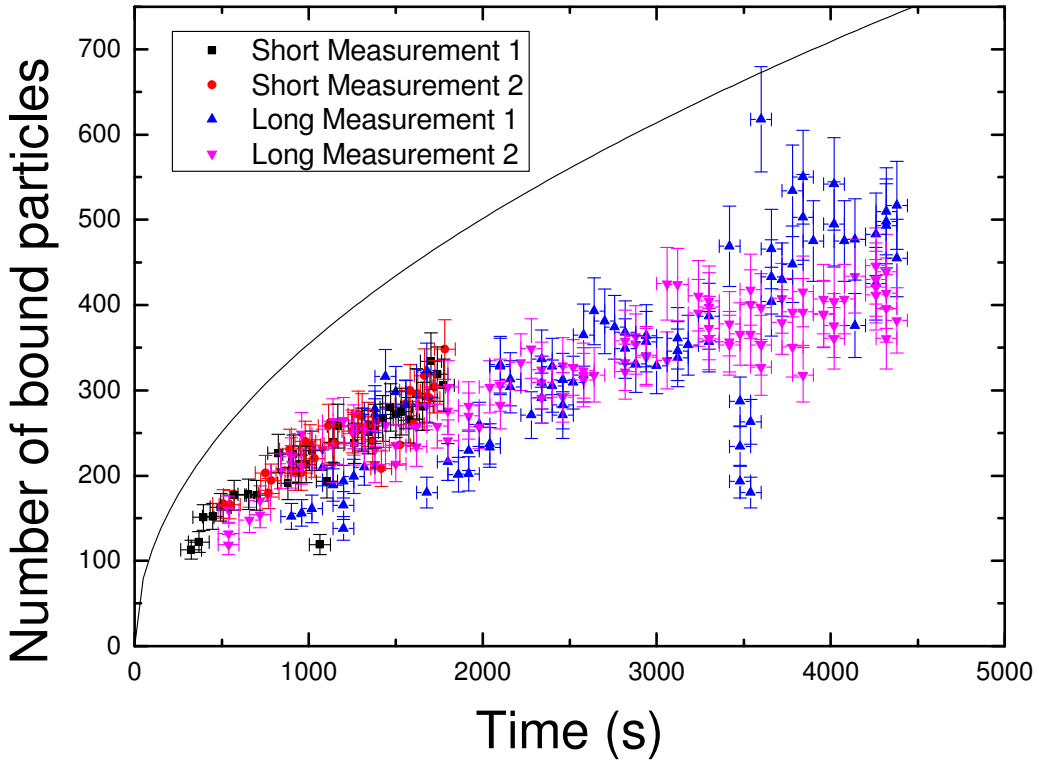

Figure 5: The number of bound particles during passive measurements as a function of time. Different colors mean measurements on different fluid cells. Error bars originate only from the analysis method. The black curve shows the number of bound particles calculated with equation 1.

The number of particles bound overlaps for most of the measurements, which means different measurements are consistent with each other. Equation 1 predicts that the number of bound particles should be a square root function of time. This is indeed the case.

For the measurement called "*Long measurement 1*" large and small values are found. The small number of particles bound can have different reasons. One possible explanation is that the measurement was done at the edge of the fluid cell. In this area,

a part of the fluid cell is not covered with streptavidin. Therefore, no particles can bind in that area. Another explanation could be that a part of the fluid cell was not coated properly with streptavidin. This causes fewer particles to bind. An explanation for the high value of particles bound could be clustering of bound particles. If these clusters are large enough, the image processing software may count them as multiple particles, resulting in a high particle count.

Equation 1 is used to calculate the number of bound particles. This is done with the following parameters. The area of the fluid cell is $1.5 * 10^{-8}$ m², the initial target concentration in the fluid cell is $7.50 * 10^{-10}$ mol/m³ (calculated by using the chemical protocol in appendix A2). The diffusion coefficient is $2.15 * 10^{-12}$ m²/s. The particle count calculated with equation 1 is shown as a black curve in figure 5. The particle count calculated with equation 1 is approximately 1.5 times higher than the experimental data. This may be caused by some incorrect parameters in the equation, like the particle concentration. The particle concentration may not be equal to the calculated value from the chemical protocol in appendix A2. This is because during the preparation of the particle solution, some fluid may be left behind in the pipette for example. This will lead to a different particle concentration than the calculated value. This possible deviation on its own cannot explain the factor 1.5 difference in particle count though. For future experiments, measuring the particle concentration in the fluid cell can be done at the start of the measurement to rule out this cause of errors.

To analyze the experimental data in more detail, simulations were performed using a numerical model. This model simulates a fluid cell filled with particles. The model calculates the number of bound particles to the bottom of the cell after a certain time. The motion of each particle is calculated individually according to Brownian dynamics. More information on the numerical model can be found in paragraph 3.4 and appendix C. The binding probability in the simulation model is set to 1, physically representing that every particle touching the reactive surface will bind to it. In figure 6 the simulated fluid cell is shown at different time steps of the simulation.

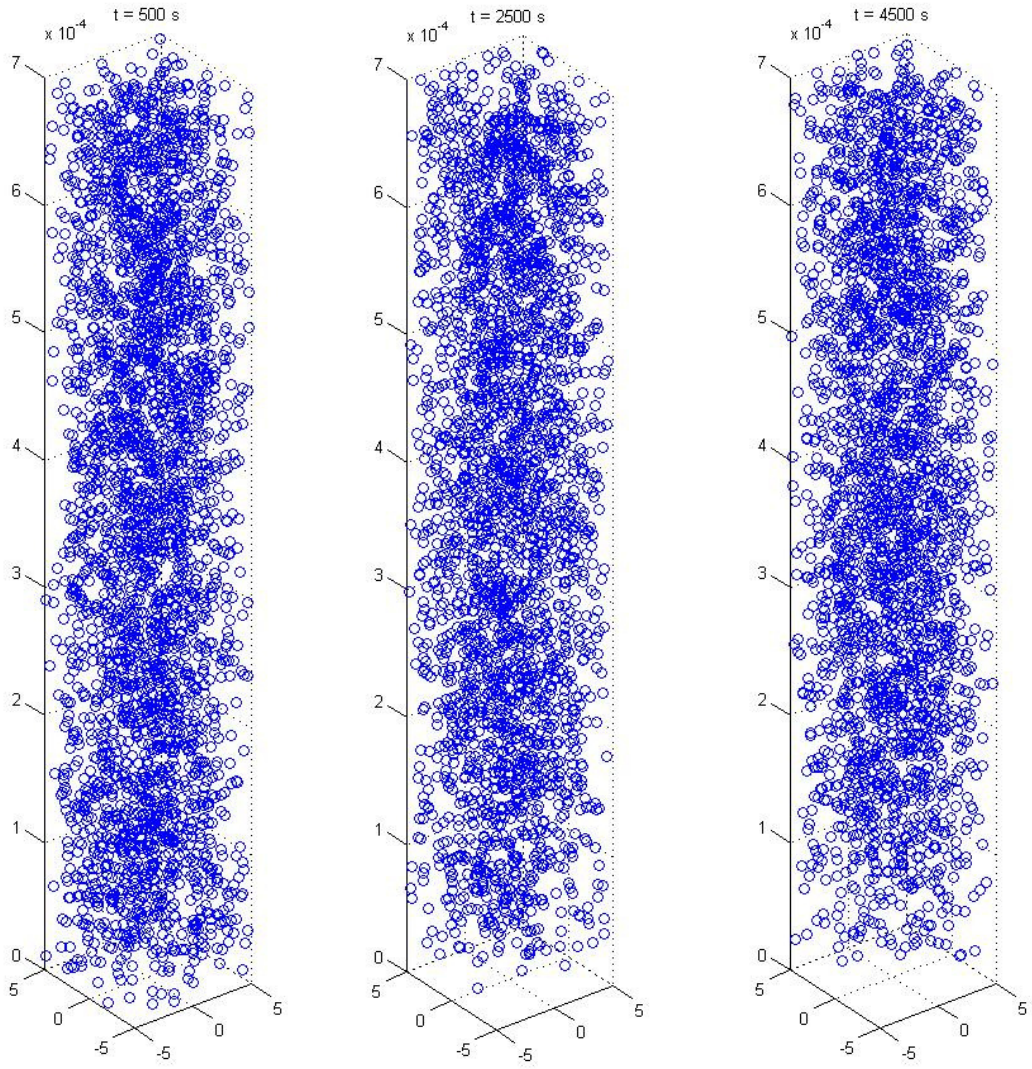

Figure 6: The simulated fluid cell at different time steps of the simulation. The figure on the left is the fluid cell at t = *500 s, the figure in the middle is made at* t = *2500 s and the figure on the right is made at* t = *4500 s. The height of the fluid cell is 700 micrometer and the length and width are both 100 micrometer.*

In figure 6 the depletion of particles at the bottom of the fluid cell is visible. The longer the simulation runs, the fewer particles will be present at the bottom of the fluid cell. The reason of this is that when particles are bound, they are removed from the simulation. Particles can only bind to the bottom of the fluid cell. That explains why depletion is only visible at the bottom of the fluid cell.

The simulation model calculates the number of bound particles after a certain time. The results are shown in figure 7.

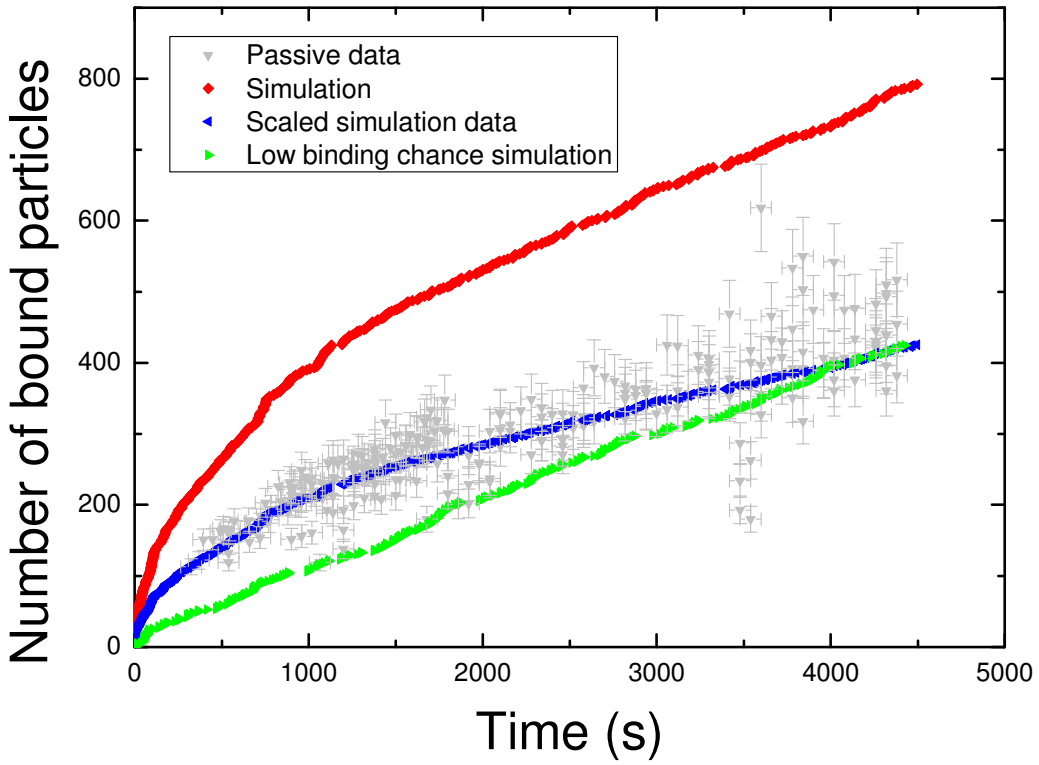

Figure 7: The number of particles bound as a function of time. The data of the passive measurements is displayed in light gray. The red data points originate from a simulation where the parameters are based upon the parameters in the real fluid cell. The binding probability in the simulation model is set to 1 for this curve. The red data points are scaled down to match the experimental data, this leads to the blue points. The green points originate from a simulation with the parameters based upon the parameters in the real fluid cell, but this time the binding probability is set to 0.01.

The red line in figure 7 originates from a simulation where the simulation parameters are based upon the parameters in actual fluid cells (the parameters are mentioned in paragraph 3.4). The binding probability in this simulation is set to 1.

As shown in figure 7, the simulation yields values approximately 1.7 times higher than the experimental data (shown in light gray) for the number of bound particles. This may be caused by a too large particle concentration in the simulation model. Scaling the simulation data down to match the experimental data yields the blue line in figure 7. This line matches the square root behavior of the experimental data.

Other simulations were performed to verify whether the large values for the particle count were caused by an incorrect binding probability in the simulation model. It is found that for a binding probability of 0.01 the simulation data matched the experimental data at t = 4500 s. This is the green data in figure 7. The green data shows linear behavior however, in comparison to the square root behavior of the experimental data. Therefore, it can be concluded that a binding probability of 1 in the simulation model is not the only reason for the large values. Whether the binding probability of 1 is correct cannot be concluded from these results, but only lowering the binding probability does not lead to correct results.

4.2 Chain dynamics during actuation

In this paragraph the dynamics of the chains during actuation in a vertical rotating magnetic field are characterized. The dynamics are studied by looking at movies made with the microscope when stirring takes place in the fluid cell.

The parameters that where studied are the average chain length, clustering of chains and whether the chains stay close to the surface during actuation.

The chain dynamics are characterized for different actuation protocols. In the first series of protocols, the magnetic field strength is varied. For the second series of protocols, the magnetic field frequency is varied. The number of bound particles during these actuation protocols is shown in the next paragraph. This paragraph will be used there to provide an explanation for the particle counts.

4.2.1 Chain dynamics when varying magnetic field strength

The theory in paragraph 2.2 shows that for a single chain in a bulk fluid in a rotating magnetic field the chain length increases with the magnetic field strength (the Mason number decreases). This is because if the magnetic field strength is increased, the dipole-dipole interactions keeping the chains together become larger in comparison to the hydrodynamic drag of the fluid on the chains (see paragraph 2.2).

In the following measurements the influence of the magnetic field strength is studied by measuring the average chain length for different magnetic field strengths. The experimental situation is different from the theoretical situation discussed in paragraph 2.2 though, because there are many chains as opposed to one. This may lead to interactions between the chains. Another difference is that chains were located on the bottom of the fluid cell during actuation and not in the middle of a fluid. This may lead to interactions between the chains and the surface.

To measure the average chain length during actuation, videos of 25 seconds are made of the rotating chains for different field strengths. At 10 different frames (2.5 s, 5.0 s, 7.5 s, …, 25 s) of the video the length of at least 5 chains (up to 10, depending on how many chains were in focus) is measured. The average chain length is then calculated from all these chain lengths. The average chain length for different field strengths is shown in figure 8. Error bars originate from using the image analysis software. The field frequency during these measurements is 0.2 Hz.

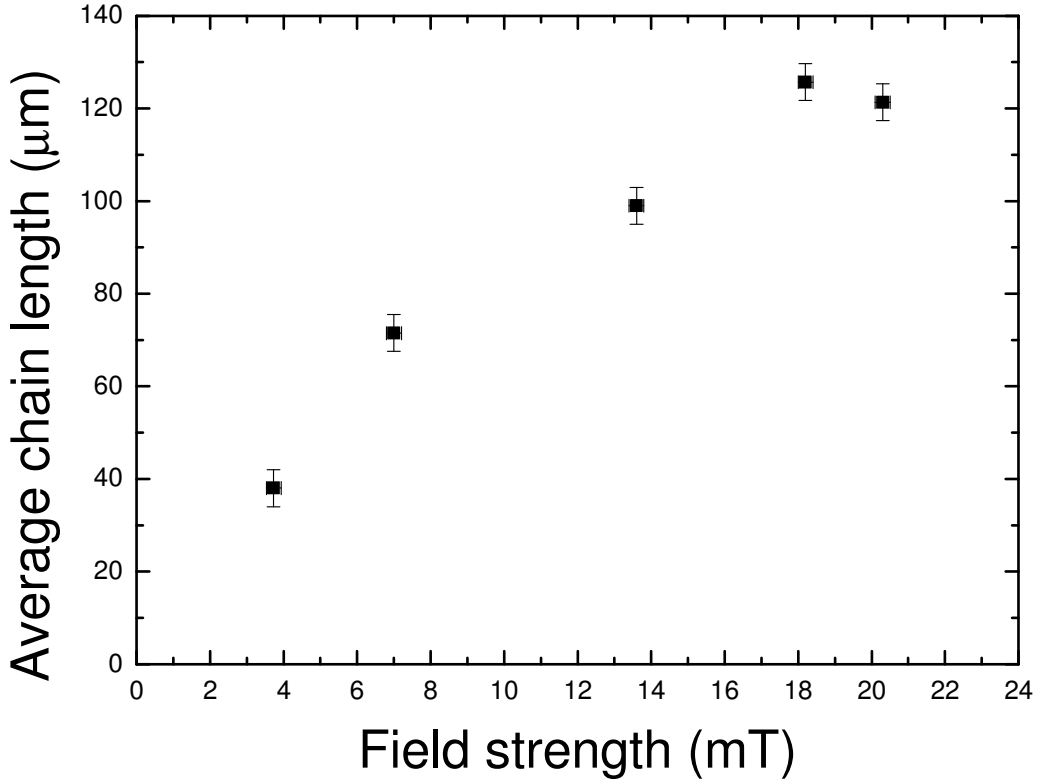

Figure 8: Average chain length of the chains of magnetic particles during actuation for different magnetic field strengths.

As shown in figure 8, it is found that the average chain length increases with the field strength. At the largest field strength (20.3 mT), clustering of the chains was visible. Clustering of chains leads to a lower average chain length. An example of clustering of chains during the measurement at 20.3 mT (taken at t = 125 s) is shown in figure 9.

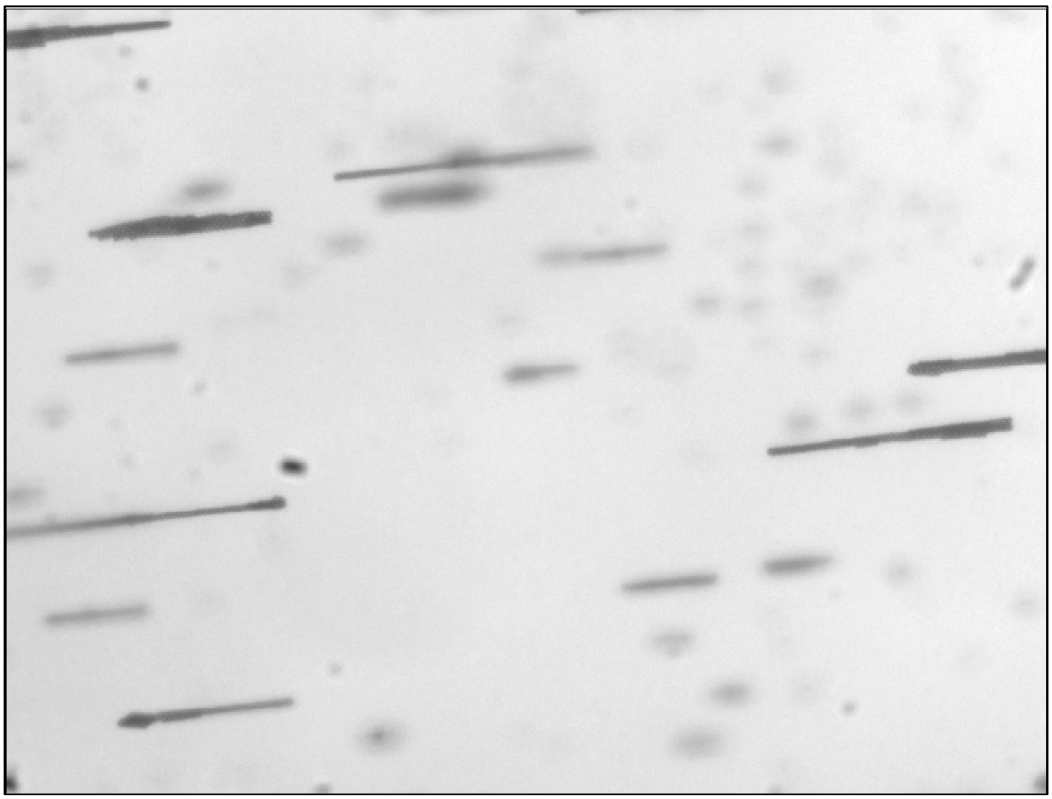

Figure 9: Clustered chains at t = *125 s during the measurement at 20.3 mT. The dimensions of the picture are 520 x 400 μm.*

A general observation from the movies was that the chain length varied more when the field strength is increased. For low field strengths, chains did stay on the surface, but from 18 mT and above, chains were also positioned more above the surface.

4.2.2 Chain dynamics when varying magnetic field frequency

Another parameter for which the dynamics of rotating magnetic chains was studied was the frequency of the rotating magnetic field. Based on equation 2 (see paragraph 2.2), a rotating chain in an unbound medium will exhibit more breaking behavior, i.e. break up in smaller chain fragments, at increased field frequencies. By increasing the frequency of the rotating field, the hydrodynamic drag on the particles is increased and only shorter chains can sustain the applied torque. Here, we studied the influence of the rotation frequency of an out-of-plane rotating magnetic field on an ensemble of particles which have sedimented on a surface. To characterize the particle behavior, movies of 25 seconds of actuated particles were recorded and the chain-length of at least 5 chains (up to 10, depending on how many chains were in focus) was determined at 10 different frames (2.5 s, 5.0 s, 7.5 s, …, 25 s). The results are shown in figure 10. The field strength during these measurements is 18.2 mT.

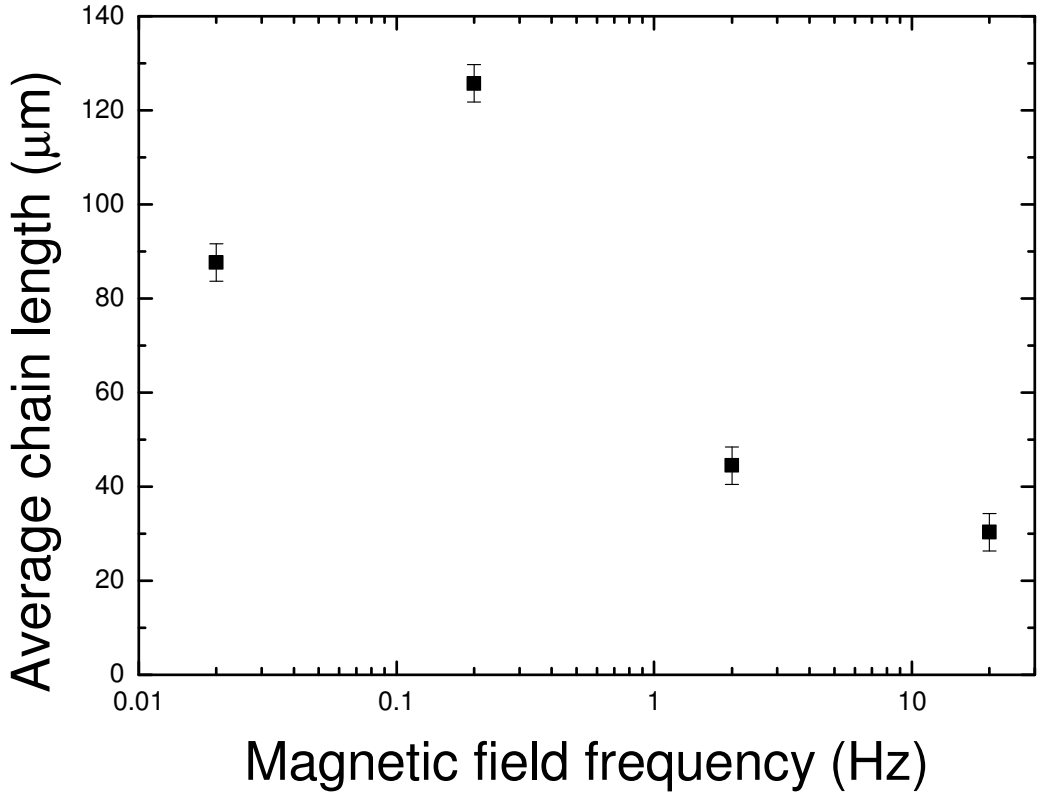

Figure 10: Average chain length of the chains of magnetic particles during actuation for different magnetic field frequencies.

For higher frequencies, it is found that chains become smaller, as shown in figure 10. The average chain length at 0.02 Hz is an exception though. At this field strength, chains were clustered together. Clustering leads to smaller chains, as was also shown in the field strength measurements. An image of the clustered chains, taken at t = 125 s, is shown in figure 11.

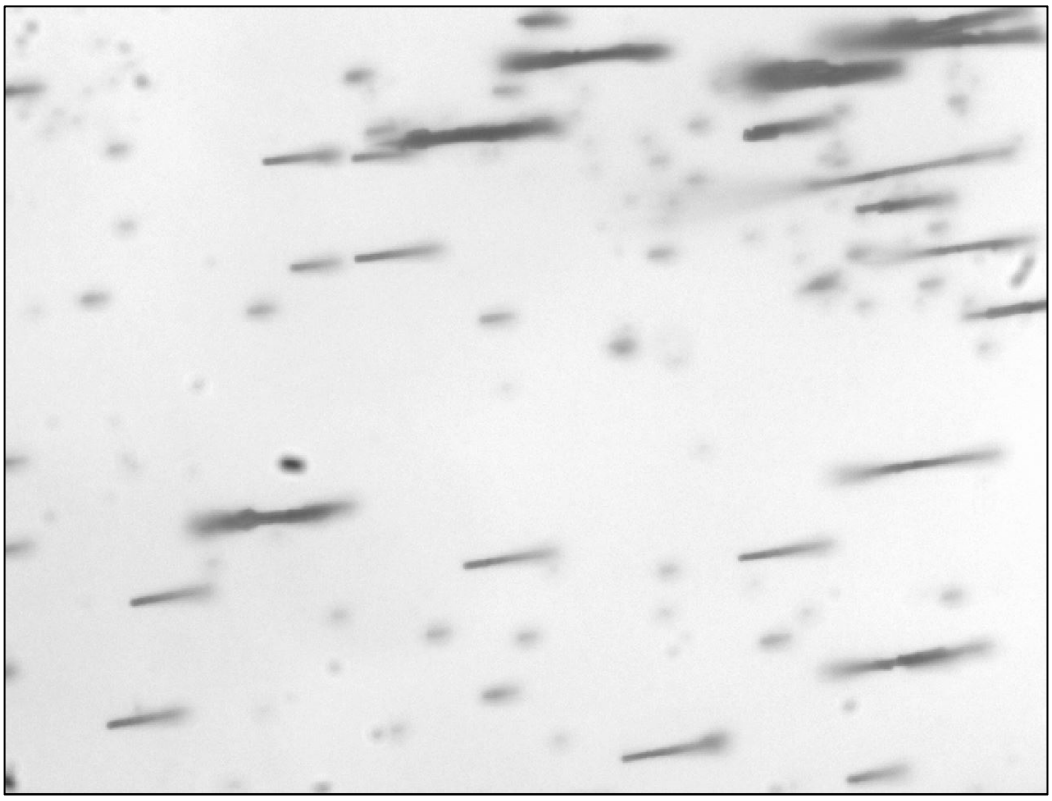

Figure 11: Clustered chains at t = *125 s during the measurement at 0.02 Hz. The dimensions of the picture are 520 x 400 μm.*

At the highest field frequency (20 Hz), chains started 'walking' over the surface rapidly. This could be seen in the videos because the chains were moving quickly to the side.

For field frequencies lower than 2 Hz the chains did not stay on the surface for the entire duration of the measurement. For 2 Hz and higher frequencies the chains did stay on the surface.

A general observation was that the chains did differ more in length when the average chain length was higher. This result is consistent with the behavior seen from the field strength measurements.

4.2.3 Time dependency of the chain length

In this paragraph, it is studied how the chain length changes as a function of time for a timescale of 250 seconds. The same out-of-plane rotating magnetic field which actuates an ensemble of particles which have sedimented on a surface is used as in paragraph 4.2.1 and 4.2.2. To characterize the time dependency of the chain length, movies of 250 seconds of actuated particles were recorded and the chain-length of 4 chains was determined at 7 to 9 different frames (there are approximately 30 seconds between the frames). Measurements were performed at a magnetic field frequency of 0.2 Hz. The measurements were performed at different field strengths: 3.73, 7.00 and 13.6 mT. The results are shown in figure 12. Error bars are caused by measuring the chains with the image analysis software.

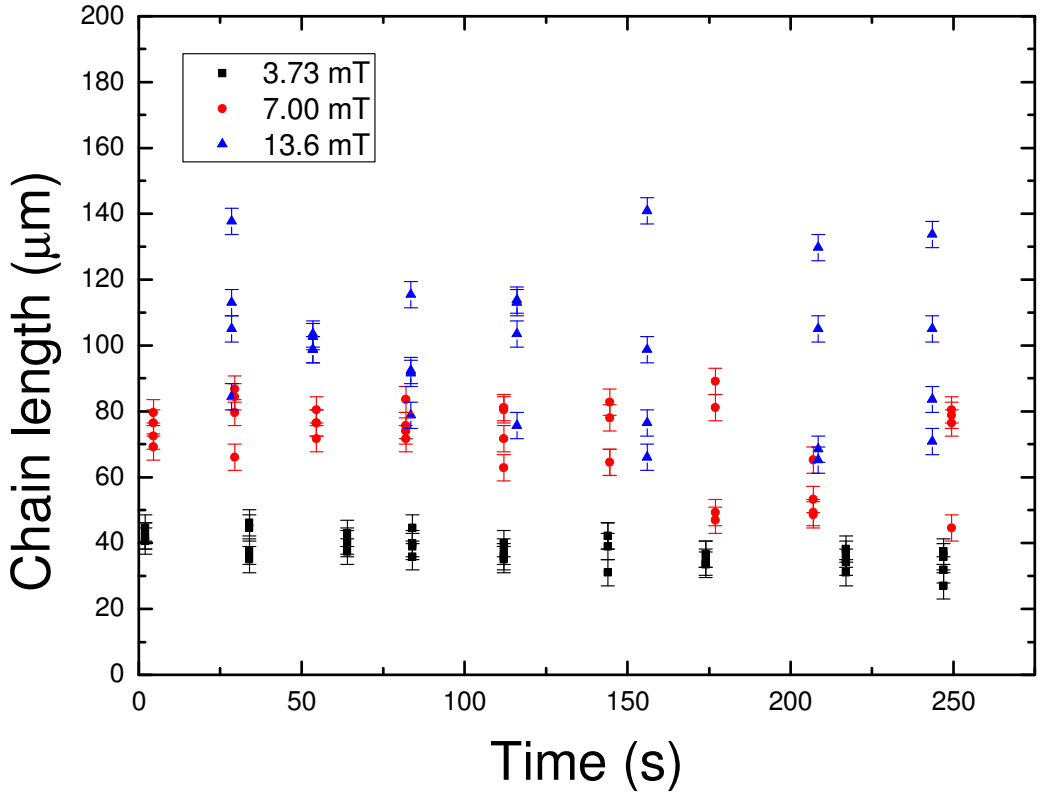

Figure 12: The chain length as a function of time. All measurements are performed at a magnetic field frequency of 0.2 Hz.

The chain length measured at 3.73 mT stays around 40 micrometer for the entire 250 seconds. The measurement at 7.00 mT shows there are larger differences in chain length than the measurement at 3.73 mT. These differences in length are smaller at t = 5 seconds than later data points. It is not possible to draw any conclusions from this however, since the sample of four measured chains is too small for this. At a field strength of 13.6 mT, the largest differences in chain length are visible.

Any other time dependency, for example an increase of the chain length as a function of time, was not found.

4.3 Capture measurements

This paragraph discusses the main results of this project. Here, the number of bound particles to the bottom of the fluid cell is presented as a function of time for various actuation protocols. Measurements are done in the following way.

First, a fluid cell is prepared according to appendix A2. After that, the fluid cell is placed in the magnetic setup, where one actuation protocol is performed. After the actuation protocol is finished (this takes 7-8 minutes), the fluid cell is placed under the microscope. Then, 7 pictures are taken with the microscope from random spots within the fluid cell. After these pictures are taken, the fluid cell is placed in the

magnetic setup again and the same actuation protocol is applied. For each fluid cell, the actuation step is carried out 3 times. This will produce 3 series of 7 images for each fluid cell.

The parameters that were varied for the different actuation protocols are the magnetic field strength and the magnetic field frequency. The actuation protocols applied in this paragraph are the same as the actuation protocols used in paragraph 4.2. By varying the magnetic field strength and field frequency, chains will show different behavior, as discussed in paragraph 2.2.

4.3.1 Varying magnetic field strength

The results of the capture measurements where the magnetic field strength was varied are shown in figure 13. The field frequency during these measurements is 0.2 Hz. The number of particles is measured at 3 time steps (1000, 2200 and 3300 s), because actuation takes place between these time steps and no measurements can be performed during actuation.

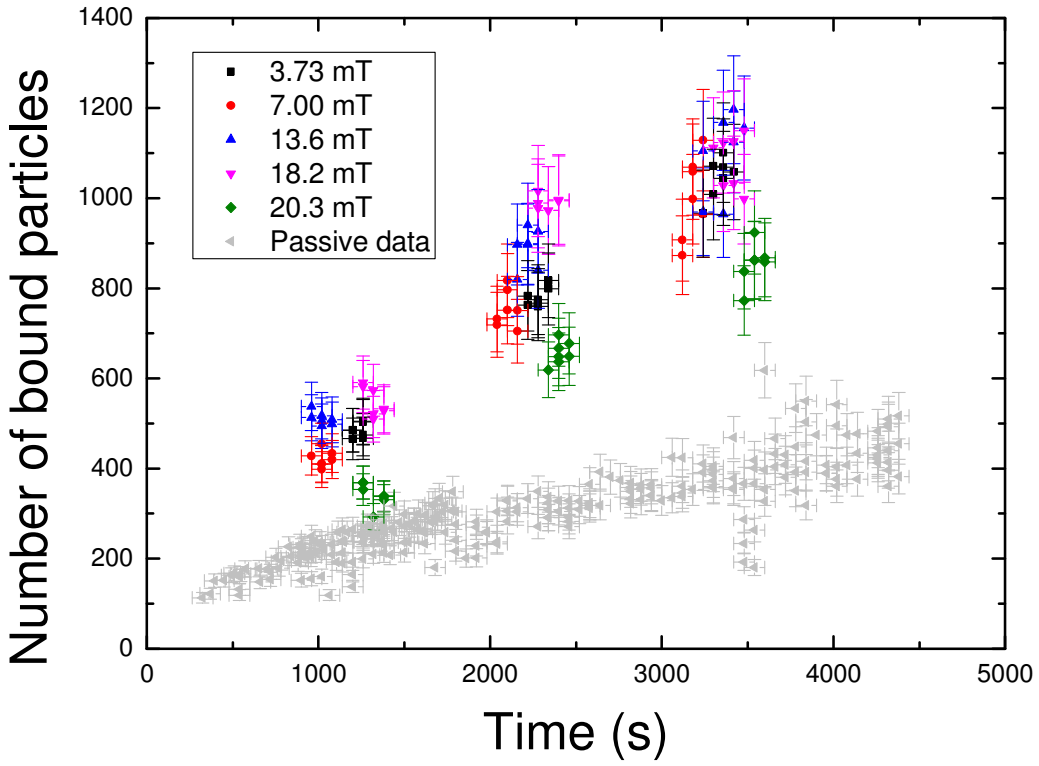

Figure 13: The number of particles bound as a function of time for different field strengths.

As shown in figure 13, more particles bind when magnetic stirring is applied. Around 1000 s, 2.1 times more particles bind when stirring as compared to the passive measurements. At 2200 seconds, 2.7 times more particles bind and at 3300 s 2.7 times more particles bind. This shows that stirring is indeed a way to speed up target capture times.

The number of particles bound does not differ significantly for different field strengths, except for 20.3 mT. At the highest field strength, the least particles bind. This can be caused by clustering of the chains at that field strength (as seen in paragraph 4.2.1). Clustering of chains does influence the stirring efficiency negatively.

The stirring efficiency is roughly the same for different field strengths, but the average chain length is not the same for these measurements (see paragraph 4.2.1). Different chain lengths should lead to different stirring efficiencies, because larger chains can stir a larger subvolume of the fluid cell. A possible explanation for the behavior in figure 13 can be that the maximum stirring efficiency is already achieved for the field strength of 3.73 mT. In this case, the binding speed of the target particles to the surface of the fluid cell may be the limiting factor.

The influence of changing the average chain length is also studied in the simulation model (discussed in paragraph 3.4 and appendix C). The chain length is a parameter in the simulation model and thus can be changed. In the simulation model, changing the chain length changes the size of the subvolume that is mixed. Stirring in the simulation model is simply redistributing particles in the stirred subvolume randomly at certain time steps to homogenize the particle concentration. More detailed information on the simulation model is shown in appendix C. The simulation model calculated the number of bound particles after a certain time. The results are shown in figure 14 for different chain lengths. The time interval of stirring is set to 20 seconds for the simulations.

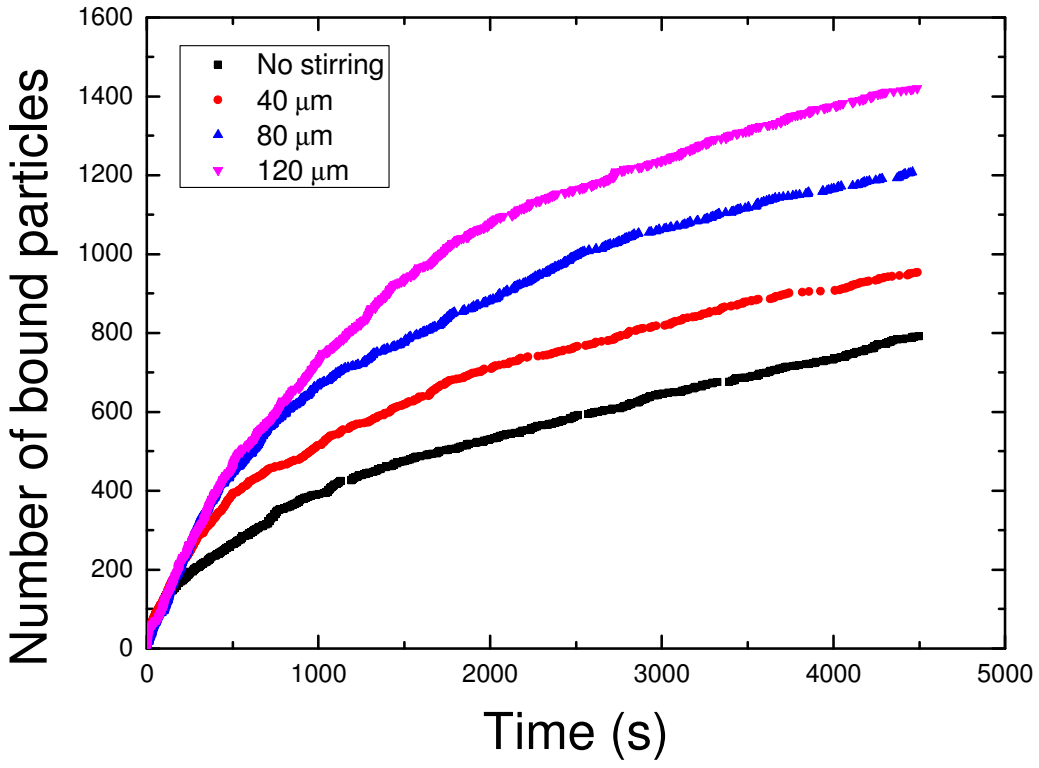

Figure 14: Number of bound particles as a function of time as predicted by the simulation model for different chain lengths. The binding probability is set to 1 for these simulations.

The simulation model predicts that for larger chain lengths more particles will bind. Around 4000 seconds, 730 particles are bound when no stirring takes place, 900 particles are bound for a chain length of 40 μm, 1160 particles for a chain length of 80 μm and 1375 particles for a chain length of 120 μm. In the experimental data, no change in the number of particles bound was found however for different chain lengths. The difference in the particle count between experimental data and the simulation model can be explained because the binding speed in the simulation model is infinitely high. Therefore, this cannot limit the number of particles that bind, unlike during the experiments.

What also is shown in figure 14 is that stirring will not be effective directly (at $t = 0$ s). For the first 200 seconds all data almost overlaps. The following explanation is found for this behavior. When the fluid gets depleted because particles are binding, the concentration will become lower at the bottom of the fluid cell than in the bulk of the fluid. A lower concentration at the bottom of the fluid cell means a larger concentration gradient between the bottom and the bulk of the fluid cell. So what happens is that stirring causes the concentration gradient to become smaller in a faster way than when only diffusion is present. Therefore, more targets will be present at the bottom of the fluid cell when stirring, as compared to the case when no stirring is applied. This will in turn lead to a higher binding speed. The first 200 seconds in figure 14, around 190 particles are bound for all cases. The concentration gradient in the fluid is still small however, causing stirring to have no visible effect. When more particles are bound, the concentration gradient will become larger, thus causing stirring to have a greater effect.

4.3.2 Varying rotational speed of magnetic field

The results for the capture measurements where the field frequency was varied are shown in figure 15. The field strength during these measurements was 18.2 mT. The number of particles is measured at 3 time steps (1000, 2000 and 3300 s), because actuation takes place between these time steps and no measurements can be performed during actuation.

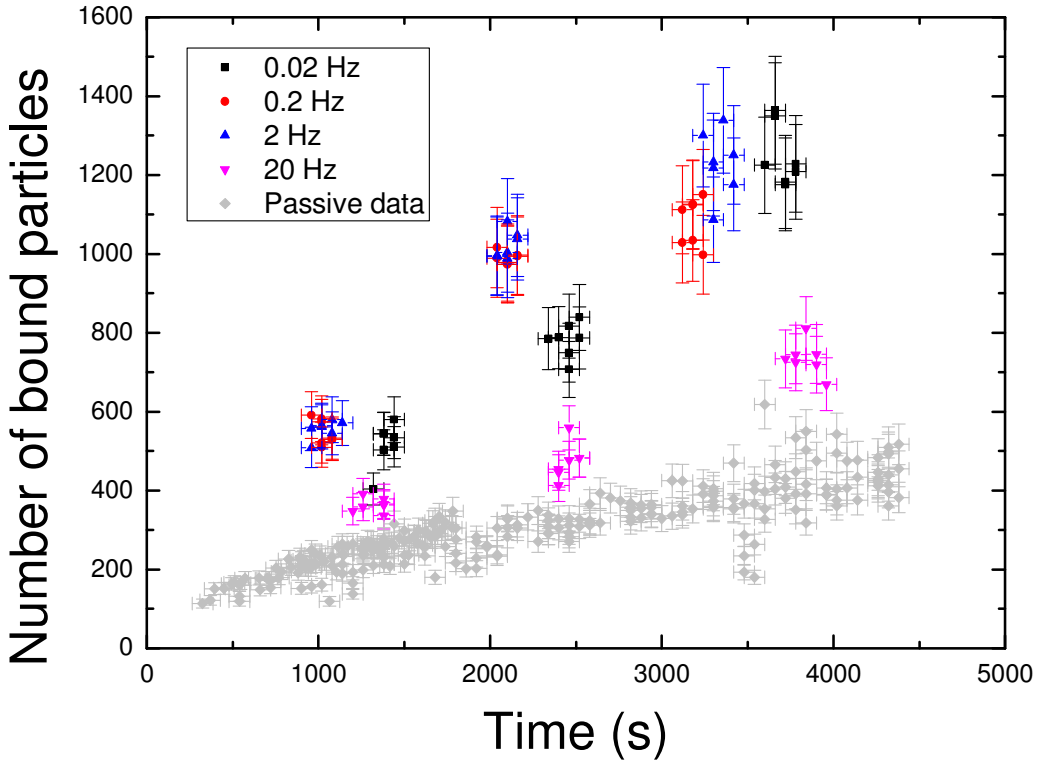

Figure 15: The number of particles bound as a function of time for different field frequencies.

In figure 15, it is shown that stirring does indeed increase the number of particles that bind. At 1000 s, 2.5 more particles bind (at 0.2 and 2.0 Hz) when stirring as compared to the passive measurements. At 2000 s, 3.1 times more particles bind when stirring and at 3300 s 3.0 times more particles bind.

The number of bound particles for 0.2 Hz and 2 Hz is almost the same. For the smallest frequency, 0.02 Hz, fewer particles bind (no numbers can be given since the measurements were not performed at the same time) and the least particles bind when the frequency is 20 Hz. The fewer particles at 0.02 Hz are caused by clustering of chains (as seen in paragraph 4.2.2). Clustering of chains decreases the stirring efficiency. This was also shown in the field strength measurements.

The data for 20 Hz can be explained by studying the chain behavior in the movie made with the microscope. At 20 Hz, the chains move quickly during actuation, because they 'walk' over the surface. This causes the chains to all move to one spot and not stir the fluid anymore. This leads to a lower stirring efficiency, which can be seen in figure 15.

The average chain length is different for 0.2 and 2 Hz (see paragraph 4.2.2). At 0.2 Hz, the average chain length is about 120 µm and at 2 Hz the average chain length is around 40 µm. Larger chain lengths lead to a higher stirring efficiency, as does a higher field frequency. It is possible that the higher efficiency because of chain length, but lower efficiency because of stirring frequency at 0.2 Hz, leads to the same number of particles bound as for 2 Hz. What also can be the case is that the maximum

stirring efficiency is already achieved and the binding speed of the targets to the surface becomes the limiting factor, just as for the field strength measurements.

5 Conclusion and outlook

The goal of this project was to study the effect of different stirring methods on the binding speed of target particles in a biosensor. Measurements were performed on a model system that consisted of a fluid cell filled with biotin-coated fluorescent particles. These particles could bind to the bottom surface of a fluid cell, which was coated with streptavidin. To overcome diffusion limitations, superparamagnetic particles (Dynaparticles-M270) were actuated by a vertically rotating magnetic field, which causes these particles to line up in chains and homogenize local fluid layers. To quantify the effectiveness of this approach, the number of targets bound to the surface was studied for different actuation protocols.

The two parameters that were varied for different kinds of stirring were the magnetic field strength and the rotational frequency of the magnetic field. To allow a more in-depth analysis of the results, the chain behavior during stirring was characterized. Furthermore, the binding process was modeled numerically by using Brownian dynamics. In the model, particles are randomly distributed across the fluid cell and the movement of each particle in time is calculated. The number of particles bound to the bottom of the fluid cell was counted. To implement magnetic stirring in the numerical model, a simplified approach was applied: when stirring takes place, the particles in a subvolume of the fluid cell are distributed randomly again. This way, the concentration gradient of the particles is made smaller, just like what happens when stirring in the real fluid cell.

First, the number of bound particles was measured as a function of time when no magnetic stirring was applied. The results found here showed the same square root dependence on the time as follows from analytically solving the diffusion equation. However, the number of bound particles was a factor 1.5 times lower than theoretically expected values. An explanation for this could be that the particle concentration entered in the analytical expression is higher than in reality. This may be partly caused by errors during the production of the target particle solution, though this cannot explain the factor 1.5 difference. The numerical model also calculated that the number of bound particles increases with the square root of time. Calculated values are a factor 1.7 higher than experimental data however. Some incorrect parameters in the simulation model, like the particle concentration, may be a reason for these high values.

After that, actuated measurements were performed. For these measurements, superparamagnetic particles were added to the fluid cell and placed in a vertically rotating magnetic field. For the actuated experiments, the number of bound particles was measured as a function of time for different actuation protocols. The parameters that were varied for the actuation protocols are the magnetic field strength and the rotational frequency of the magnetic field.

If the number of bound particles during the actuated measurements is compared to the number of bound particles during the passive measurements, an increase can be seen for the number of bound particles when actuating. The factor more particles bound when actuating varied from 2.1 to 3.1. From these results, it can be concluded that magnetic stirring indeed causes an increase in binding speed for target particles.

When varying the magnetic field strength, almost the same amount of particles was bound for each field strength, except for the highest field strength (20.3 mT). The lower amount of particles binding at 20.3 mT is caused by the chain behavior: at this field strength the chains form clusters, which decreases the stirring efficiency. The lack in difference of stirring efficiency for the other field strengths can be explained because the maximum stirring efficiency may already be achieved at the lowest field strength. Increasing the field strength does increase the chain length, but if the binding speed of the particles to the surface becomes the limiting factor, increasing the stirring volume by creating larger chains would have no effect.

If the rotational frequency of the magnetic field is varied, the number of bound particles stays almost the same for every field frequency. At the lowest frequency (0.02 Hz), fewer particles bind because of clustering of the chains. At the highest frequency (20 Hz), the least particles bind however. When looking at the chain behavior, it is shown that the chains move rapidly to one of the magnetic poles at 20 Hz. This is because they start 'walking' over the bottom surface of the fluid cell. This way, the chains will not be dispersed over the entire surface and this will lead to a lower stirring efficiency. The lack of difference in particle count for the other field frequencies can again be explained because the maximum stirring efficiency may already be achieved at the lowest field frequency. Another explanation could be that a low frequency leads to larger chains, thus increasing the stirring efficiency, but at the same time decrease the stirring efficiency because the chains rotate slower. These two opposing effects on the stirring efficiency could compensate each other and in this way produce no difference in particle count during the measurements.

For the actuated measurements done during this project, a change in magnetic field strength or field frequency did not lead to a change in the binding speed of particles. This may be because the maximum stirring efficiency is already achieved in that case. For future experiments, it can be studied if this is indeed the case by lowering the stirring efficiency. This can be achieved by measuring at lower field strengths for example. This would reduce the size of the chains and in this way reduce the stirring efficiency. Another solution is measuring with different particles. These particles can be either smaller in size or have a smaller magnetic susceptibility. Both of these solutions will lead to smaller chains, which will reduce the stirring efficiency. Another solution may be to use shorter actuation protocols.

6 References

1. T. G. Kang et al., Chaotic mixing induced by a magnetic chain in a rotating magnetic field, Physical Review E (2007) 4-5.

2. Srisa-Art et al., Monitoring of Real-Time Streptavidin-Biotin: Binding kinetics using droplet microfluidics. Anal. Chem. (2008) 80: 7063-7067.

3. Grassia et al., Journal of Fluid Mechanics (1995).

Appendices

Appendix A1: Protocol for coating fluorescent polystyrene particles with biotin

Necessary materials:

- PBS tablets (Phosphate Buffered Saline)
- MES (2-(N-Morpholino)ethanesulfonic acid)
- BSA (Bovine serum albumin)
- Demineralized water (demi water)
- Sodium Azide
- EZ-Link Amine-PEG3-Biotin (Thermo scientific, Pierce)
- Carboxylate modified fluorescent particles (a 2% solid suspension of carboxylate modified polystyrene particles from Invitrogen), 200 nm size
- EDC (N-(3-Dimethylaminopropyl)-N'-ethylcarbodiimide hydrochloride)
- Ethanolamine

Necessary equipment:

- Vortex mixer
- Thermo mixer
- Sonicator finger

Buffers/solutions:

- 200 mL PBS buffer: 5 mM PBS in demi water.
    - Dissolve 1 PBS tablet in 200 mL demi water.
- 5 mL MES buffer: 50 mM MES in demi water, pH value 5.
    - Take 53.31 mg MES.
    - Dissolve the MES in 5 mL demi water.
- 5 mL ethanolamine: 50 mM ethanolamine in demi water (can be created during step 7 of the protocol).
- 10 mL storage buffer: Dilution of 1 mg BSA/mL (can be created during step 7 of the protocol).

Protocol:

1. Add 500 µL of the fluorescent particle solution to a 1.5 mL eppendorf tube (tube A).
2. Add 450 µL of the MES buffer to tube A.
3. Add 50 µL of Amine-PEG3-Biotin to tube A.
4. Take another 1.5 mL eppendorf tube (tube B) and add 2.88 mg of EDC to it.
5. Add the contents of tube A to tube B.
6. Make the suspension homogenous by using a vortex mixer. If agglomeration occurs, use the sonicator finger to disperse the fluorescent particles.
7. Let the suspension incubate for 2 hours at room temperature using the thermo mixer at 1400 rpm.
8. Add 100 µL ethanolamine solution.

9. Incubate the solution 30 minutes at room temperature in the thermo mixer (1400 rpm).
10. Centrifuge the solution for 30 minutes and remove the supernatant with a pipette.
11. Add 500 µL of the PBS buffer and suspend the coated fluorescent particles by using the sonicator finger.
12. Repeat step 10 and 11 seven times.
13. Add storage buffer to the tube so that the total content is 500 µL.

Appendix A2: Protocol for preparing the fluid cells for measurements

Necessary materials:

- Streptavidin
- Biotin coated fluorescent particles (FB)
- Polystyrene coverslips
- Fluid reaction chamber sticker
- Fluid cell
- PBS tablets (Phosphate Buffered Saline)
- MES (2-(N-Morpholino)ethanesulfonic acid)
- BSA (Bovine serum albumin)
- Demineralized water (demi water)
- **ONLY when actuated measurements are required:**
- M270 carboxyl magnetic particles (MP)

Necessary equipment:

- Tweezers
- Microscope
- In case of actuated measurements: magnetic setup

Buffers/Solutions:

- 200 mL PBS buffer: 5 mM PBS in demi water.
  - Dissolve 1 PBS tablet in 200 mL demi water.
- 15 mL MES buffer: 50 mM MES in demi water. The pH should be 6.2 ± 0.3.
  - Take 159.93 mg MES.
  - Dissolve the MES in 15 mL demi water.
- 750 µL Streptavidin (100 µg/mL): Streptavidin (10 mg/mL) diluted 100 times.
  - Take 10 µL 10 mg/mL streptavidin and add 190 µL MES buffer.
  - Of the 200 µL streptavidin and MES, take 150 µL and add it to a new eppendorf tube.
  - Add 600 µL MES to the solution in the new eppendorf tube.
- 15 mL BSA/PBS block buffer. A PBS solution containing 10 mg BSA/mL.
  - Take 150 mg BSA.
  - Add 15 mL PBS.
- FB solution: 2 ppm (~7.6 pM) FB
  - Take 10 µL FB.

- Add 990 µL BSA/PBS block buffer.
- From this dilution, take 10 µL in a new eppendorf tube.
- Add 990 µL BSA/PBS block buffer.
- **Following steps ONLY when actuated measurements are required:**
- Take 200 µL of this dilution in a new eppendorf tube.
- Add 1.6 µL MP.

Protocol:

1. Take an Agar polystyrene coverslip.
2. Clean in isopropanol, then in ethanol. Dry with air.
3. Place a fluidic reaction chamber sticker (peel of the paper side) on the coverslip.
4. Repeat step 1-3 in case of multiple fluid cells.
5. Add 90 µL streptavidin on all coverslips. Make sure the streptavidin is spread out over the entire surface.
6. Incubate overnight (~18 hours) at room temperature.

The next day:

7. Take the streptavidin of the fluidic reaction chamber.
8. Wash the fluidic reaction chamber once using 100 µL PBS buffer.
9. Peel the plastic layer of the fluid cell and put it on top of the fluidic reaction chamber sticker.
10. Add 100 µL BSA/PBS block buffer.
11. Incubate 1 hour at room temperature.
12. Remove the block buffer with a pipette.
13. Wash the fluid cell with the BSA/PBS block buffer 4 times.
14. Prepare the microscope and the camera software for measurements. This ensures measurements can be immediately started when targets are present in the fluid cell.
15. Remove the BSA/PBS block buffer from the fluid cell and add 50 µL of the FB solution. Make a note of the current time as reference point $t = 0$ during the measurements with the microscope.
16. Seal of the fluid cell with small plastic stickers.
17. The fluid cell can now be placed under the microscope or in the magnetic setup for measurements.

Appendix B: Analyzing data with ImageJ

The tool used to analyze pictures and movies taken with the camera on the microscope is imaging process software ImageJ (version 1.46r). This appendix will provide the settings that are used to analyze the data with and give an explanation why these settings are used.

The steps used in ImageJ to calculate the number of bound particles from a microscope picture are as follows.

- File → Import → Image Sequence

    - Select the desired images
- Process → FFT → Bandpass Filter
    - Filter large structures down to 40 pixels
    - Filter small structures up to 1 pixels
    - Suppress stripes: none
    - Tolerance of direction: 5%
    - Check 'Autoscale after filtering' and 'Saturate image when autoscaling'
- Image → Adjust → Threshold
    - Set threshold to 125
    - Use black and white values
    - Check 'Dark background'
    - Press 'Apply'
- Analyze → Analyze Particles
    - Size: 4 - 100
    - Circularity: 0.00 – 1.00
    - Show: nothing
    - Check 'Summarize'
    - Press 'OK'

After pressing OK in the last step, a table is shown with the number of counted particles of all the imported images in the second column.

Tuning some of the parameters greatly influences the number of bound particles as an outcome. The influence of the following parameters on the number of bound particles was studied: the value of the threshold during the 'Threshold' step and the particle size during the 'Analyze Particles' step.

The lower limit of the particle size is chosen to be 4 pixels. This is to prevent noise from being counted as a particle, but with this value small particles will still be counted.

The influence of changing the threshold is studied by measuring the number of bound particles in one microscope image with different thresholds. This is done at different lower limits for the particle size (chosen during the 'Analyze Particles' step). The results are shown in figure 16.

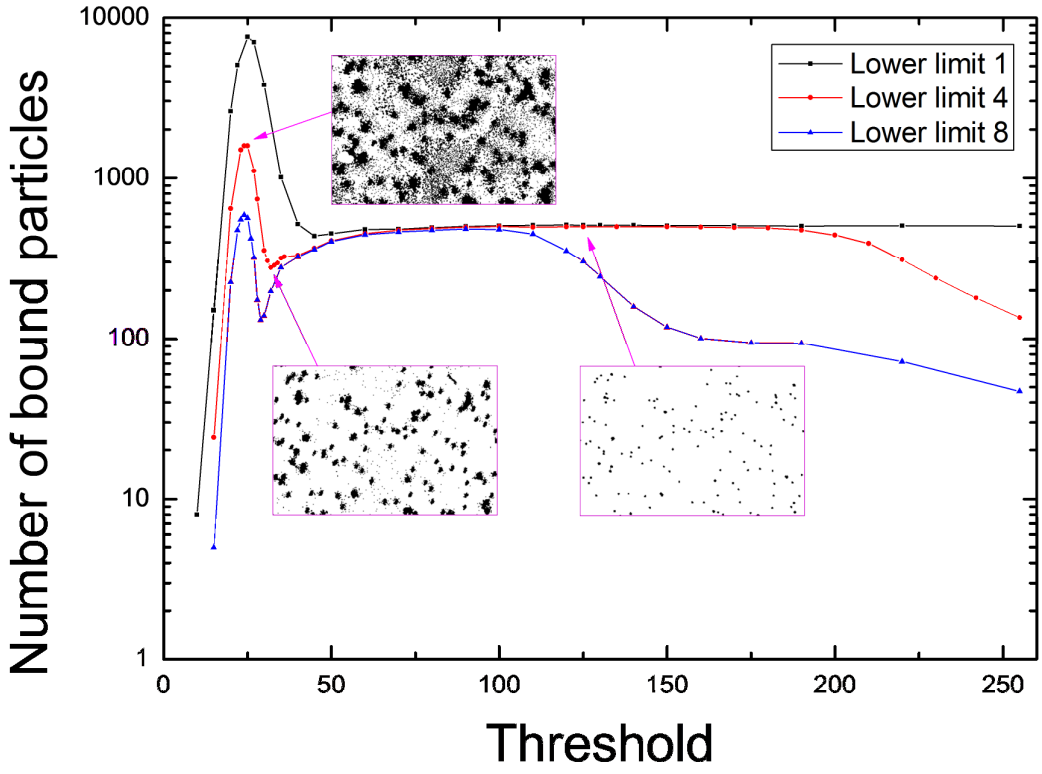

Figure 16: Influence of different values of the threshold on the particle count. Different colored lines indicate a different lower particle limit during the 'Analyze Particles' step. Three microscope images during image processing are inserted into the graph.

Figure 16 shows that for threshold values around 15 and lower very few particles (around 10) are counted. This is because such a low threshold causes the image to become very dark. Increasing the threshold value rapidly causes more counted particles, up to thousands of particles. This is because a lot of noise will become visible at threshold values around 30 (as shown in figure 16). The software will treat some of this noise as particles. For threshold values around 40, a local minimum in the number of bound particles is found. This is caused by multiple particles being connected together. This will lead to larger but fewer particles. For threshold values of 50 and higher, the particle count will stay constant. If the measured particle count is compared to the particles counted on the original microscope picture by hand, it is shown that the particle count found after image processing is in the right order of magnitude. For very high thresholds (200 and above) every particle in the image will start to vanish. This causes less bound particles for very high threshold values.

The threshold at the center of the plateau shown in figure 16 is chosen as threshold to use during the experiments. Since the chosen lower limit is 4, the threshold chosen is 125. The difference in particle count between the threshold 75 and 125 and between 125 and 175 is approximately 10%. For other images, the optimal threshold may have a different value though. If we assume the chosen threshold is still on the plateau however, we can say the uncertainty in the particle count is 10%. This way, it is not necessary to find the optimal threshold for each analyzed image.

Another parameter that was studied was the upper limit of the particle size during the 'Analyze Particles' step. To determine the right value for this, a series of images is analyzed with different upper limits for the particle size. The results are shown in figure 17.

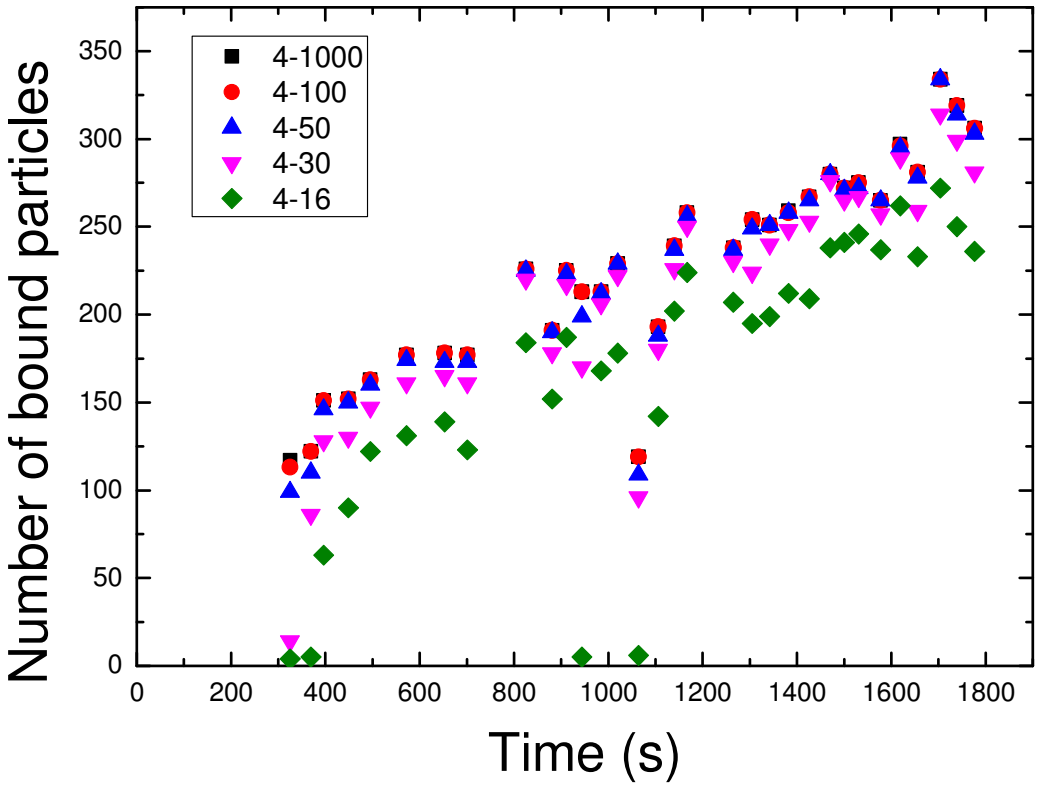

Figure 17: The number of bound particles for a series of microscope images. Different colors indicate different upper limits of the particle size. The lower limit of the particle size is 4 pixels in all cases.

As shown in figure 17, the number of bound particles generally increases when the upper limit for the particle size is increased. This is because more particles will qualify to be counted when the upper limit is increased. Based on figure 17, an upper limit of 100 pixels is chosen. This is because the number of bound particles found with the analysis matches the number of bound particles in the pictures counted by hand. Increasing the upper limit above 100 pixels is not necessary, because there are no larger particles present in the microscope pictures. As shown in figure 17, this is indeed the case. If the upper limit is increased to 1000, no more particles will be counted than when the upper limit is 100 pixels.

Appendix C: Matlab code used in simulations

In this appendix the Matlab code used in simulations is shown. In the first part of the code, called 'initialization', simulation parameters can be changed. Some of these simulation parameters include the particle concentration, the dimensions of the

simulated fluid cell, the simulation time and the binding probability of target particles to the surface.

Parameters important for stirring are the chain length, the position of the chains in the fluid cell and how often stirring takes place.

In the next part of the code the motion of the particles is calculated. This is done for each particle individually according to Brownian dynamics. If a particle is bound to the bottom of the fluid cell or not is also determined in this part of the code. When a particle is assigned a negative z-coordinate (to the bottom of the fluid cell), it qualifies for binding. Depending on the binding probability, the particle may bind. If it binds, the particle is removed from the simulation. If it does not bind, the particle is bounced back into the fluid cell.

In the part of the code called 'stirring part' the stirring process is performed. If stirring is turned on, a subvolume (with the same height as the chain length) of the fluid cell will be stirred. Stirring in this model is simply distributing the particles in the stirring volume randomly across the stirring volume. This stirring process takes place each 20 seconds. This time can be edited by changing the parameter 'stirring_interval' in the first part of the code. Stirring in this way is a simplification of the situation when stirring in a real fluid cell. In reality, stirring with magnetic chains would cause a flow and this would influence the number of particles that bind. Stirring at the surface may even make the bound particles at the surface unbound again. The general result of stirring however is that the particle concentration is homogenized in the stirring area. This simulation model does just that, it simulates the results of stirring. Keep in mind though that stirring in the simulation model is simplified compared to stirring in a fluid cell in reality.

The boundary conditions applied in the next part of the simulation can be described as follows. When a particle is placed above the fluid cell, it is bounced back against the top of the fluid cell. If a particle is placed x units to the right of the right side of the fluid cell, it will be placed x units to the right of the left side of the fluid cell. The same holds for when a particle is moved to the left of the fluid cell. This way, the length and width of the fluid cell are treated as infinitely high.

The last part of the code produces two figures. In the first figure the fluid cell is displayed with the particles in it. This figure will update during the simulation and therefore show the movement of the particles. The second figure is produced at the end of the simulation. In this figure the number of bound particles is shown as a function of time.

```
clear all
clc
close all
global deltat R k kk initialangle yup

%%%%%%%%%%%%%%%%%%%%%%
%% initialization %%%
%%%%%%%%%%%%%%%%%%%%%%

deltat=0.1;          % timestepsize
```

```
deltaz=1E-9;          % stepsize; maybe not needed
hmax=700E-6;          % height of chamber
width=100E-6;         % width of chamber
Rtarget=100E-9;       % initially neglegt this as it effectively
increases MP radius
Conc=7.49549003E-13;          % target concentration in mol/dm^3 (this
is 1 pM)
eta=0.001;            % dynamic viscosity
T=293;                % Kelvin
tmax=4500;            %s later ophogen naar een uur (dan ook deltat
naar 0.1)
var=0.288675;
% var=0;                          %%% if Brownian motion is undesired
BindProbability=1;                % 0.01 geeft waarden die overeenkomen
met meetdata
stirring=0;                       % 1 = on, 0 = off, only used to
initialize
chain_length=120E-6;              % meter
stirring_height=10E-6;            % lower limit where stirring takes
place
stirring_interval=20;             % each ... seconds stirring will take
place
hstart=0E-6;



%%% constants
Navo=6.022E23;        % mol^-1
kb=1.38065E-23;

%%% computed quantities
Volume=hmax*width^2;              % in m^3
TargetNumber=round(Conc*1000*Volume*Navo);  % 1000*mol/dm^3*m^3*Navo
==> ~90 for 0.1 pM

%%% initialization of targets
PosTarget=rand(TargetNumber,3);      % random filling: 1 = x, 2 = y, 3
= z
PosTarget(:,1)=PosTarget(:,1).*width-0.5*width;
PosTarget(:,2)=PosTarget(:,2).*width-0.5*width;
PosTarget(:,3)=PosTarget(:,3).*(hmax-hstart)+hstart;




%%%%%%%%%%%%%%%%%%%%%%%%%%%%%%%%%%%%%%%%%%%%%%%%
%% calculating movement of targets alone%%%
%%%%%%%%%%%%%%%%%%%%%%%%%%%%%%%%%%%%%%%%%%%%%%%%
path1=zeros(tmax/deltat+1,1); path1(1)=PosTarget(5,2);
track2=1;
Capttrack=zeros(1,2);
Captured=0;
Stirred=0;

for t=deltat:deltat:tmax
    track2=track2+1;

DispTarget=deltat.*((1./(6.*pi.*eta.*Rtarget)).*normrnd(0,var,[Target
Number-Captured,3])*sqrt(6*pi*eta*Rtarget*24*kb*T/(deltat)));
    PosTarget=PosTarget+DispTarget;
```

```
    %%% Determine bound particles
      check=1;
    while check==1

        [minpos,entry]=min(PosTarget(:,3));
        if minpos <=0
           if rand<=BindProbability
               Captured=Captured+1; Capttrack(Captured+1,1)=t;
Capttrack(Captured+1,2)=Captured;
               PosTargetnew=zeros(TargetNumber-Captured,3);
               PosTargetnew(1:entry-1,:)=PosTarget(1:entry-
1,:);                                              % can handle
negative entry=1
               PosTargetnew(entry:TargetNumber-
Captured,:)=PosTarget(entry+1:TargetNumber-Captured+1,:);    % can
handle negative entry=last
               PosTarget=PosTargetnew;
           else             %perform reflecting boundary condition
               PosTarget(entry,3)=abs(PosTarget(entry,3));
           end
        else
           check=0;
        end
    end

    %%
    %%% stirring part %%%

    % use the following if statement to turn stirring on and off

     if mod(t,stirring_interval)==0
         stirring=1;                    % 1 = on, 0 = off
     end



    if stirring==1

        TargetNumber_st=0;
        for i=1:1:TargetNumber-Captured

            if PosTarget(i,3)<=stirring_height+chain_length &&
PosTarget(i,3)>=stirring_height      %filter out targets that will be
stirred
                TargetNumber_st=TargetNumber_st+1;
                Stirred=Stirred+1; %Stirredtrack(Stirred+1,1)=t;
Stirredtrack(Stirred+1,2)=Stirred;  %for tracking purposes
            end

        end
        clear i;


        %%%%generate new coordinates for after stirring
        PosTarget_st=rand(TargetNumber_st,3);     % random filling: 1
= x, 2 = y, 3 = z
```

```
        PosTarget_st(:,1)=PosTarget_st(:,1).*width-0.5*width;
        PosTarget_st(:,2)=PosTarget_st(:,2).*width-0.5*width;

PosTarget_st(:,3)=stirring_height+PosTarget_st(:,3).*chain_length;

        %%%assign the new coordinates

        j=1;

        for i=1:1:TargetNumber-Captured

            if PosTarget(i,3)<=stirring_height+chain_length &&
PosTarget(i,3)>=stirring_height      %filter out targets that will be
stirred
                PosTarget(i,1)=PosTarget_st(j,1);
                PosTarget(i,2)=PosTarget_st(j,2);
                PosTarget(i,3)=PosTarget_st(j,3);
                j=j+1;
            end

        end
        clear i,j;



    end

    %%
    %%% boundary conditions
%     PosTarget(:,3)=mod(abs(PosTarget(:,3)),hmax);%&upper boundary
condition: reflective
    PosTarget(:,3)=hmax-abs(-PosTarget(:,3)+hmax);%&upper boundary
condition: reflective
    PosTarget(:,1)=mod(PosTarget(:,1)+width/2,width)-width/2;%side
boundary condition: continuous
    PosTarget(:,2)=mod(PosTarget(:,2)+width/2,width)-width/2;%side
boundary condition: continuous
    if mod(t,10)==0   %0.1 ophogen wellicht
        figure(1);
        scatter3(PosTarget(:,1),PosTarget(:,2),PosTarget(:,3));axis
equal;   %  DEZE MISSCHIEN MINDER FREQUENT MAKEN
    end
    xlim([-0.5*width 0.5*width]);ylim([-0.5*width 0.5*width]);zlim([0
hmax])
    path1(track2)=PosTarget(5,2);


end
figure(4); scatter(Capttrack(:,1),Capttrack(:,2));
```

Appendix D: Derivation of expression for the number of bound particles

As starting point, the diffusion equation (also known as Fick's second law) is used.

$$\frac{dp}{dt} = D\frac{d^2p}{dx^2} \tag{3}$$

Where $p(x,t)$ is the concentration of the diffusing particles in particles/m³, t the time in seconds, D the diffusion coefficient in m²/s and x the position in m, in our case the height of the fluid cell, where $x = 0$ is located at the bottom of the fluid cell.

Also, the following boundary conditions are used.

$$p(x,0) = \text{Heavyside step function} \tag{4}$$

$$p(0,t) = 0 \tag{5}$$

Equation 4 is used to set the starting condition for the particle concentration. At $t = 0$ no particles are bound to the bottom of the fluid cell yet and therefore the particle concentration is the same everywhere in the fluid cell. This assumes that particles are distributed evenly across the fluid cell at $t = 0$.

Equation 5 is used to make sure the solution for $p(x,t)$ does not get a constant term (see also equation 6).

To solve equation 3, the following solution is tried.

$$p(x,t) = A\,\mathrm{erf}(z) \tag{6}$$

With A an arbitrary constant and erf(z) the error function of z. The error function is defined in equation 7.

$$\mathrm{erf}(z) = \frac{2}{\sqrt{\pi}}\int_0^z e^{-y^2}dy \tag{7}$$

The derivative of the error function is given in equation 8.

$$\frac{d\mathrm{erf}(z)}{dz} = \frac{2}{\sqrt{\pi}}e^{-z^2} \tag{8}$$

Now both $\frac{dp}{dt}$ and $\frac{d^2p}{dx^2}$ are determined.

$$\frac{dp}{dt} = A\frac{d\mathrm{erf}(z)}{dt} = A\frac{dz}{dt}\frac{d\mathrm{erf}(z)}{dz} = A\frac{dz}{dt}\frac{2}{\sqrt{\pi}}e^{-z^2} \tag{9}$$

$$\frac{d^2p}{dx^2} = A\frac{d^2\,\mathrm{erf}(z)}{dx^2} = \mathrm{A}\frac{d}{dx}\left(\frac{dz}{dx}\frac{d\mathrm{erf}(z)}{dz}\right) = \mathrm{A}\frac{d}{dx}\left(\frac{dz}{dx}\frac{2}{\sqrt{\pi}}e^{-z^2}\right)$$

$$= A\left(\frac{d^2z}{dx^2}\frac{2}{\sqrt{\pi}}e^{-z^2} + \frac{2}{\sqrt{\pi}}\frac{dz}{dx}\frac{dz}{dx}\frac{de^{-z^2}}{dz}\right) = A\left(\frac{d^2z}{dx^2}\frac{2}{\sqrt{\pi}}e^{-z^2} - 2z\frac{2}{\sqrt{\pi}}\frac{dz}{dx}\frac{dz}{dx}e^{-z^2}\right) \tag{10}$$

The derivatives can now be substituted in equation 3.

$$A\frac{dz}{dt}\frac{2}{\sqrt{\pi}}e^{-z^2} = DA\left(\frac{d^2z}{dx^2}\frac{2}{\sqrt{\pi}}e^{-z^2} - 2z\frac{2}{\sqrt{\pi}}\frac{dz}{dx}\frac{dz}{dx}e^{-z^2}\right) \quad (11)$$

$$\frac{dz}{dt} = D\left(\frac{d^2z}{dx^2} - 2z\frac{dz}{dx}\frac{dz}{dx}\right) \quad (12)$$

In the equation above, $\frac{d^2z}{dx^2}$ is treated as equal to zero. This is because z is assumed to be proportional to x. Therefore, the second derivation to x is zero.

Equation 12 then becomes equation 13.

$$\frac{dz}{dt} = -2Dz\frac{dz}{dx}\frac{dz}{dx} \quad (13)$$

Now z is written as $z = X(x)T(t)$. This leads to equation 14.

$$\frac{1}{T^3}\frac{dT}{dt} = -2D\left(\frac{dX}{dx}\right)^2 \quad (14)$$

The left side of equation 14 only depends on t, the right side only on x. Therefore, if t is varied, the right side of the equation does not change. The same can be said for varying x and the left side of the equation. Because of this, both sides of the equation must be constant.

$$-\frac{1}{T^3}\frac{dT}{dt} = \mathrm{C} \rightarrow T = \frac{1}{\sqrt{2Ct}} \quad (15)$$

$$2D\left(\frac{dX}{dx}\right)^2 = C \rightarrow X = x\sqrt{\frac{C}{2D}} \quad (16)$$

By combining equations 15 and 16, the following expression for z is found.

$$z = X(x)T(t) = \frac{x}{\sqrt{4Dt}} \quad (17)$$

After that, Fick's first law is used at the bottom of the fluid cell to derive an expression for the particle flux per unit area there. This particle flux per unit area will be the same as the amount of particles that bind per unit area in case all particles passing the surface will bind.

$$J = -D\frac{dp}{dx} \text{ at } x = 0 \quad (18)$$

For p, the following expression is used.

$$p(x,t) = A\mathrm{erf}(\frac{x}{\sqrt{4Dt}}) \quad (19)$$

By substituting equation 19 in equation 18 and by using equation 8, the following expression is found for J.

$$J = -D\frac{d}{dx}A\,\mathrm{erf}\left(\frac{x}{\sqrt{4Dt}}\right) = -\mathrm{DA}\frac{2}{\sqrt{\pi}}\frac{d}{dx}\frac{x}{\sqrt{4Dt}} = -\frac{A\sqrt{D}}{\sqrt{\pi t}} \quad (20)$$

The minus sign for J in equation 20 indicates the particle flow is directed in the negative x direction, so particles flow downwards. For the amount of captured particles, only the absolute value of J is relevant. The amount of captured particles per unit area is calculated from equation 20 by carrying out the integral in equation 21.

$$Captured\ particles/unit\ area\ = \int_0^t |J(t')|dt' = \int_0^t \frac{A\sqrt{D}}{\sqrt{\pi t'}} dt' = \frac{A\sqrt{4Dt}}{\sqrt{\pi}} \qquad (21)$$

The A in equation was introduced in equation 6. This constant is equal to the particle concentration infinitely far away from the surface, called p_∞, times Avogadro's number. The concentration p_∞ is the same as the particle concentration in the fluid cell at time $t = 0$. The dimension of p_∞ is mol/m³. By using this information and multiplying the expression in equation 21 with the area of the fluid cell A (in m²), an expression is found for the number of captured particles in equation 22.

$$Captured\ particles = Ap_\infty N_A \sqrt{\frac{4Dt}{\pi}} \qquad (22)$$